THE JOURNAL OF PHYSICAL CHEMISTRY C

Article

pubs.acs.org/JPCC

Light-Induced Degradation of $CH_3NH_3PbI_3$ Hybrid Perovskite Thin Film

Youzhen Li,[†] Xuemei Xu,[†] Congcong Wang,[‡] Ben Ecker,[‡] Junliang Yang,[†] Jinsong Huang,[§] and Yongli Gao*[,‡]

[†]School of Physics and Electronics, Central South University, Changsha, Hunan 410083, P.R. China

[‡]Department of Physics and Astronomy, University of Rochester, Rochester, New York 14627, United States

[§]Department of Mechanical and Materials Engineering, Nebraska Center for Materials and Nanoscience, University of Nebraska—Lincoln, Lincoln, Nebraska 68588, United States

Supporting Information

ABSTRACT: The stability of $CH_3NH_3PbI_3$ was investigated by observing the degradation in a coevaporated film irradiated by a blue laser in ultrahigh vacuum. X-ray photoelectron spectroscopy (XPS) and scanning electron microscopy (SEM) were employed to investigate the effects of irradiation on the surface. The core levels of $CH_3NH_3PbI_3$ were observed to shift toward a higher binding energy (BE) during the irradiation, suggesting that the surface became more n-type. A new metallic Pb component in the XPS spectrum appeared after 120 min of irradiation, indicating that the film had started to decompose. The decomposition saturated after about 480 min of irradiation when the ratio of metallic Pb to total Pb was about 33%. Furthermore, the film was no longer continuous after irradiation, as the elements gold and oxygen from the substrate were detected by XPS. SEM images also show a roughened surface after irradiation. The results strongly indicate that $CH_3NH_3PbI_3$ is sensitive to the laser irradiation and that the light induced decomposition is a self-limiting process.

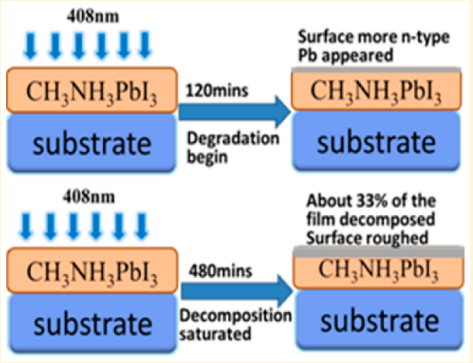

INTRODUCTION

Organic photovoltaics,[1] dye-sensitized solar cells,[2] and colloidal nanocrystal solar cells[3] have widely been investigated in recent years as an important source of renewable energy. The most critical factors for the utility of solar cells are their cost of production, power conversion efficiency (PCE), and the sustainability of the source materials. Recently, organic–inorganic halide perovskites have attracted considerable attention as a light-harvesting material for new solar cells,[4−9] offering both low cost and reasonably high PCE compared with that of silicon, dye-sensitized, and other standard solar cells. Hybrid perovskite was first used in a dye-sensitized solar cell by Miyasaka and co-workers in 2009 with a PCE of 3.8%.[10] Kim and co-workers later reported a solid-state hybrid perovskite solar cell with a PCE of 9.7% in 2012.[5] Soon after that, hybrid perovskite solar cells with a planar heterojunction structure were also reported with a PCE of 5%,[11] and have since continued to rapidly increase to as high as a certified value of 22.1%.[12] Hybrid perovskite solar cell's PCEs are presently quite close to that of the standard crystalline silicon solar cells.

Hybrid perovskite films are mainly fabricated by either solution based spin coating or thermal evaporation. The spin coating method is a simpler process and of lower production cost than that of the latter, and it is therefore popularly used for device fabrication. Surface and interface investigations of spin-cast films have produced information important for understanding the performance of devices fabricated with spin-casting.[13−17] However, the surface composition of spin coated films usually deviates significantly from the stoichiometric ratio.[18,19] Alternatively, the thermal evaporation method can produce smoother films with the correct surface stoichiometry and crystal structure,[20−22] which is essential for surface sensitive analytical investigations on the fundamental material properties of the hybrid perovskite.

Although the PCE of the hybrid perovskite solar cell has already reached over 20% in laboratory,[12] the stability of the light-harvesting film ($CH_3NH_3PbX_3$, X = I, Cl, Br) remains a critical issue for the eventual success of commercial applications. Early work attributes illumination induced degradation of hybrid perovskite solar cells to the TiO_2 layer in the device.[23] Murugadoss et al. investigated light illumination stability of thin hybrid perovskite films on different substrates and found a strong substrate dependence.[24] Bryant et al. demonstrated light illumination played a key role in hybrid perovskite degradation when exposed to gases and ambient air.[25] Applying simultaneous luminescence and electron

Received: November 25, 2016
Revised: February 6, 2017
Published: February 6, 2017

DOI: 10.1021/acs.jpcc.6b11853
J. Phys. Chem. C 2017, 121, 3904−3910

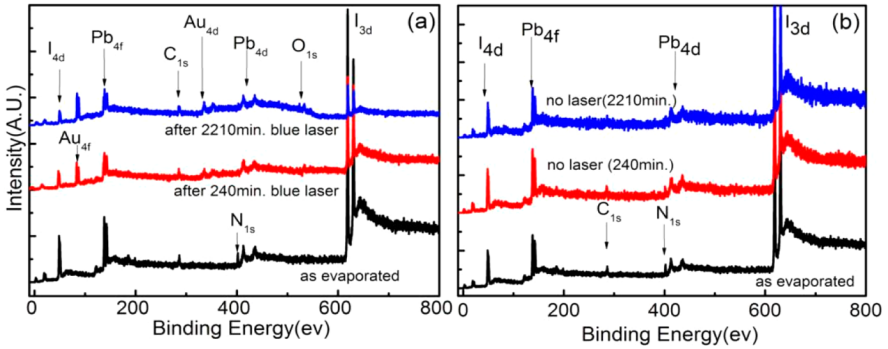

Figure 1. Survey XPS spectra of the $CH_3NH_3PbI_3$ film: (a) laser irradiated position and (b) nonirradiated position. Some substrate Au was exposed by the irradiation, and it was not seen at the nonirradiated position.

microscopy, Yuan et al. found that light-induced degradation results in material decomposition but little photoluminescent (PL) spectral shifts.[26] On the other hand, Merdasa et al. observed rapid degradation and continuous PL spectral blue shift of hybrid perovskite nanocrystals using super-resolution luminescence microspectroscopy.[27] We have previously shown that $CH_3NH_3PbI_3$ is sensitive to moisture and decomposes rapidly after reaching a threshold of 2×10^{10} Langmuir of water exposure.[22]

In this work, we present our investigation of the effects of laser irradiation on $CH_3NH_3PbI_3$ films using XPS and SEM. The films were prepared by thermal evaporation, with proper stoichiometry, uniformity, and crystal structure. After laser irradiation for only 120 min by blue light of wavelength 408 nm at intensity ~7 times of AM 1.5, a new component of Pb started to appear, marking the initiation of $CH_3NH_3PbI_3$ decomposition. The decomposition saturated after about 480 min of irradiation at the same intensity, with the perovskite Pb reduction by about 33%. The uniformity of the film was also destroyed by the irradiation as the elements from the substrate, gold and oxygen, were detected by XPS and roughening of the surface was shown by SEM. The results provide important insight for the design of hybrid perovskites-based solar cells.

EXPERIMENTAL SECTION

Film Fabrication. The film evaporation and XPS measurements were performed in a modified Surface Science Laboratories' SSX-100. The base pressure of the evaporation chamber is typically 1×10^{-7} Torr. PbI_2 (Shanghai Zhenpin Technology Co.,99%) and CH_3NH_3I (Wuhan Crystal Solar Cell Technology co.) powder were put into tungsten boats separately. Thermal couples were tightened near the center of the boats to acquire accurate temperature measurements during coevaporation. A piece of gold-coated silicon was loaded into the chamber as the substrate after cleaned with methanol. The film thickness (mass equivalent thickness) was monitored with a quartz crystal microbalance and the final film thickness was 10 nm. More details of the instrument and the evaporation procedure are described previously in ref 28.

Irradiation and XPS Measurements. The sample was then transferred into the analytical chamber of base pressure 1×10^{-10} Torr, which was equipped with an X-ray monochromator with a high-throughput bent quartz crystal providing monochromatic Al Kα radiation (1486.6 eV). The irradiation light used for exposure came from a semiconductor laser with a wavelength of 408 nm. The laser's output power was 20 mW and the irradiation intensity on the sample was about 6.8×10^{-3} W/mm^2, which was about 7 times the commonly used AM1.5 irradiation (1000W/m^2). The laser irradiation covered an oval shaped area approximately 1.4 × 2.6 mm, and the probing X-ray spot was about 0.8 × 1.4 mm in size. After each timed irradiation, we immediately performed XPS measurements on both the laser irradiated spot and another nonirradiated spot on the surface. Precise control of the sample position was guided by an optical microscope attached to the chamber. All other windows on the chamber were shaded to avoid the light influence from the outside.

Data Process and SEM Images. The valence band maximum (VBM) of the film is determined by the intersection of linear extrapolations of the leading edge and of the background. The core level peaks were fitted with commercial software Origin 6.0. Shirley-type corrections were performed to remove the secondary electron background and the ratio of Lorentzian and Gaussian line shapes was not fixed during the peak fitting. The atomic ratio of the film was calculated by comparing the areas of the fitted curves divide by their elemental sensitivity factor. At the end of the experiment for a total irradiation time of 2210 min, the sample was taken out of the chamber and was investigated immediately with a Zeiss Auriga SEM located at the University of Rochester's UR-nano center.

RESULTS AND DISCUSSION

Evidence of Degradation. Figure 1a shows the survey scan of the film before and after laser irradiation. For comparison, the scan of nonirradiated position is also shown in Figure 1b. (see Figure S1 in the Supporting Information for more survey scans) There were no other obvious elements in the as evaporated survey scan except for C, N, I, and Pb, indicating that the $CH_3NH_3PbI_3$ film was uniform and free of contamination. The atomic ratios of the as-evaporated film are N:I:Pb = 1.10:3.28:1.00 and 1.09:3.26:1.00 at the laser illuminated and nonilluminated spot, respectively. Carbon was not shown here because the contamination from the substrate was difficult to eliminate. The ratio of N:I:Pb can demonstrate a reasonably good stoichiometry. The atomic ratio also shows the surface uniformity. The polycrystallinity of the film thus prepared has been demonstrated previously.[29] As shown in Figure 1a, after only 240 min of irradiation, the Au 4f and O 1s peaks are clearly visible, indicating that the film was no longer uniform. The presence of Au and O suggests that the photoemitted electrons were coming from the underlying gold substrate, which had water or oxygen adsorbates on it because it was not sputter cleaned prior to the evaporation. At

DOI: 10.1021/acs.jpcc.6b11853
J. Phys. Chem. C 2017, 121, 3904−3910

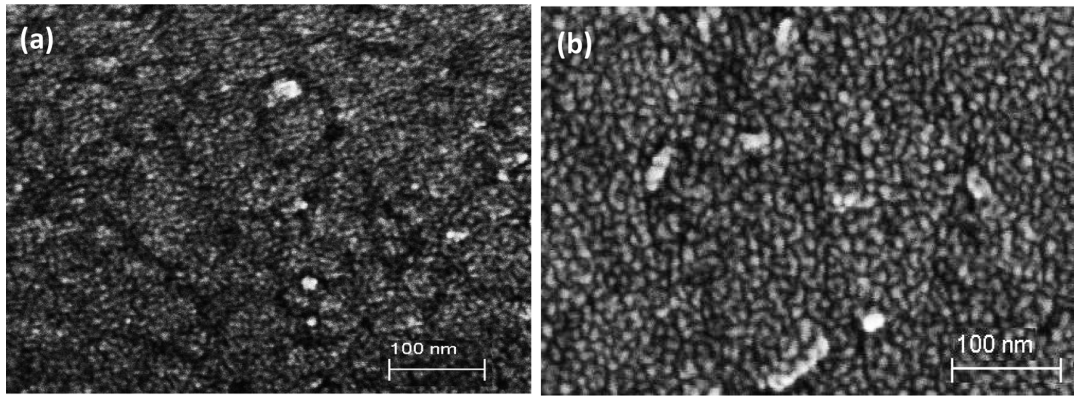

Figure 2. SEM images of the coevaporated film at (a) after 2120 min laser irradiation position and (b) nonirradiated position. The irradiated region is much rougher than the nonirradiated one.

the end of the experiment when the sample was irradiated for 2210 min, the intensity of the Au 4f and O 1s peaks further increased. In contrast, the XPS spectra from the nonirradiated position show no gold or oxygen, as can be seen in Figure 1b. The XPS survey scan results strongly suggest that the $CH_3NH_3PbI_3$ film is sensitive to laser irradiation, and the high intensity (~7 times of AM 1.5) of the laser may accelerate the degradation process. In addition, we found that after only about 120 min of laser irradiation, the color of the exposed spot became visibly lighter than that of the nonirradiated region.

Figure 2 shows the top-view SEM of the coevaporated $CH_3NH_3PbI_3$ film. Figure 2a shows the irradiated position after 2210 min of laser irradiation. It shows that the surface is clearly very rough. The small cracks created by the irradiation indicate that the film was not uniform and they are likely responsible for exposing the underlying Au substrate observed in XPS. The SEM image of the nonirradiated position shown in Figure 2b indicates the film was uniform and with a polycrystalline structure. There are some bright linear structures in the micrograph with a length of less than one hundred nanometers, which may be excessive CH_3NH_3I particles. The obvious change of the surface morphology before and after irradiation also indicates the degradation by irradiation, as the evaporated $CH_3NH_3PbI_3$ films have previously been demonstrated to be more uniform and efficient for solar cells than solution-processed ones.[9]

Detailed Analysis. In parts a and b of Figure 3, we present the valence band of the $CH_3NH_3PbI_3$ film during the experiment. Figure 3a is from the laser irradiated position, while Figure 3b is from the nonirradiated one. We found that the valence band maximum (VBM) increased by about 0.4 eV, from 0.85 eV initially to 1.25 eV after the total 2210 min of irradiation. The shift seemed to be saturated after about 480 min of irradiation. The band gap of $CH_3NH_3PbI_3$ is known to be around 1.55 eV,[17] so the "as prepared film" was a slightly n-type one to begin with. The shift toward a high binding energy (BE) indicated the film became more n-type during the laser irradiation. Meanwhile at the nonirradiated position, no obvious changes can be seen in the VBM region. Another feature to notice is that after only 120 min of laser irradiation, a new peak at about 6.5 eV begins to appear in the irradiated spectrum. This indicates the existence of oxygen on the surface, as the film is in the ultrahigh vacuum chamber and is not sensitive to oxygen exposure.[22] The oxygen could only come from contaminants on the underlying substrate since the substrate surface was not cleaned by Ar sputtering prior to

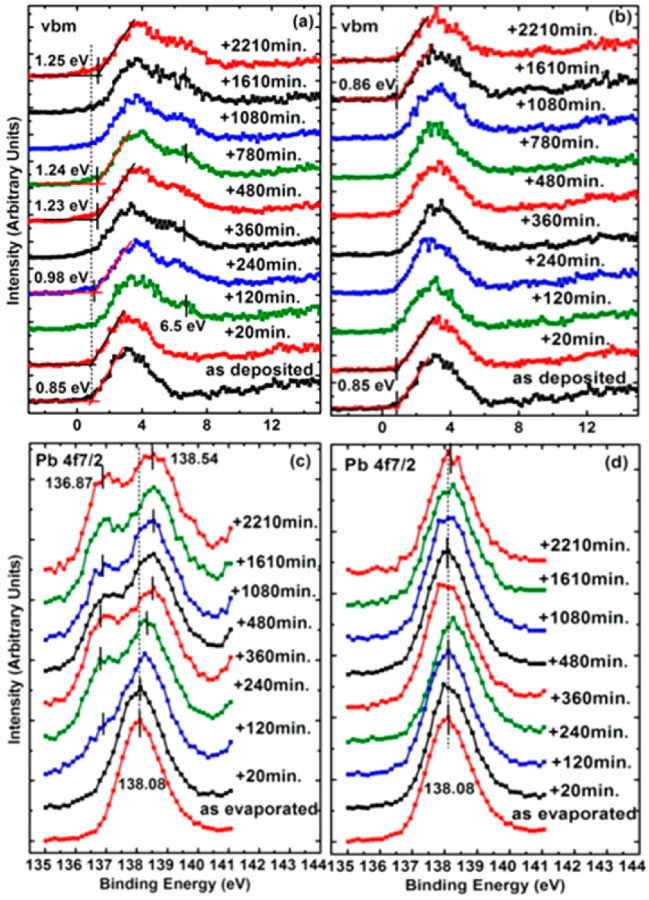

Figure 3. XPS spectra of the valence band and Pb $4f_{7/2}$ of the $CH_3NH_3PbI_3$ film at (a, c) laser irradiated positions and (b, d) nonirradiated positions. The irradiation-induced changes are clearly visible in parts a and c after the irradiation.

evaporation of the $CH_3NH_3PbI_3$ film. This further provides evidence that parts of the substrate were uncovered as photoemitted electrons from the underlying gold substrate could be seen.

Shown in parts c and d of Figure 3 are the Pb $4f_{7/2}$ spectra from laser irradiated and nonirradiated positions, respectively. The BE of as-evaporated Pb $4f_{7/2}$ is about 138.08 eV, which is consistent with the previous report.[28] As the laser irradiation progresses, changes can be observed in the core level position. After about only 120 min of laser irradiation, a new peak at

DOI: 10.1021/acs.jpcc.6b11853
J. Phys. Chem. C 2017, 121, 3904−3910

about 136.87 eV in Pb $4f_{7/2}$ began to appear (Figure 3c) and it grew in intensity as the irradiation continued. The new Pb $4f_{7/2}$ peak is that of metallic Pb, and it seems synchronized to the 6.5 eV peak in the VBM region. In contrast, the Pb $4f_{7/2}$ spectra of the nonirradiated position shown in Figure 3d present no discernible spectral changes.

$CH_3NH_3PbI_3$ films are usually known to decompose into PbI_2 and other components.[21,29] PbI_2 is photosensitive and can usually decompose into PbO and I_2 in the presence of moisture and light.[30] In our case, the film was in ultrahigh vacuum-(UHV), where there was no H_2O or oxygen. It is apparent that the PbI_2 released by laser irradiation further decomposes into metallic lead and iodine by irradiation alone, leading to the new peak in Pb $4f_{7/2}$ at 136.87 eV as shown in Figure 3c. Iodine released in this photochemical reaction will sublimate to vacuum, leaving the metallic Pb with the remaining hybrid perovskite. Previous reports have also found metallic lead in as fabricated $CH_3NH_3PbI_3$ films (especially for spin-cast films), and it was considered to be related to the excessive precursor PbI_2 and the removal of I_2.[18] The binding energy of metallic Pb is reported to be 137.0 eV,[31−33] which is very close to that of the new component at 136.87 eV after irradiation. The metallic lead will act as quenching centers of excitons, evidenced by the detrimental effect it has on the photoluminescence quantum efficiency.[33] As a result, this degradation process will have a serious effect on the device PCE. On the other hand, the degradation process may be kinematically limited in the bulk of hybrid perovskite or in a well sealed device when the volatile components in the reaction are not allowed to escape as easily as in a vacuum.

Beside the decomposition, we also found an ∼0.46 eV shift of perovskite Pb $4f_{7/2}$ from 138.08 to 138.54 eV in the irradiated position (see Figure 3c). This shift of the perovskite Pb $4f_{7/2}$ is consistent with that of the VBM, supporting the notion that the film has become more n-doped. The n-doping may be due to the fact that the film has become Pb rich, similar to the case when a hybrid perovskite is annealed at high temperature.[18]

Further support of the n-doping of the $CH_3NH_3PbI_3$ film can be obtained by observing the shifts of the other core levels. Should there be n-doping, the movement of the Fermi Level within the band gap toward the conduction band minimum will result in a rigid shift in all the energy levels in the semiconductor. The evolution of I $3d_{5/2}$ and N 1s at laser irradiated (Figure 4, parts a and c) and nonirradiated (Figure 4, parts b and d) position are both shown in Figure 4 to have a comparison. Dotted lines and short bars are marked to show the core level shift. For the laser irradiated position, the I $3d_{5/2}$ had a ∼ 0.51 eV shift (Figure 4a) toward higher binding energy from 618.97 to 619.48 eV after the irradiation. The shift also seems to be already saturated after 480 min of irradiation. A similar shift can also be seen for N 1s in Figure 4c. The shift is about the same as that of Pb $4f_{7/2}$ considering the instrument uncertainty. We can thus conclude that these shifts in the core levels were caused by the movement of the Fermi level in the film, which is further consistent with the VBM shift shown in Figure 3a. We also found a serious intensity decrease of N 1s after irradiation shown in Figure 4c, indicating the decomposition of the film and the escape of N. For the nonirradiated position, such shifts were again not observed (Figure 4, parts b and d).

Mechanism of Degradation. On the basis of the above discussions, we found that the results agree with a mechanism

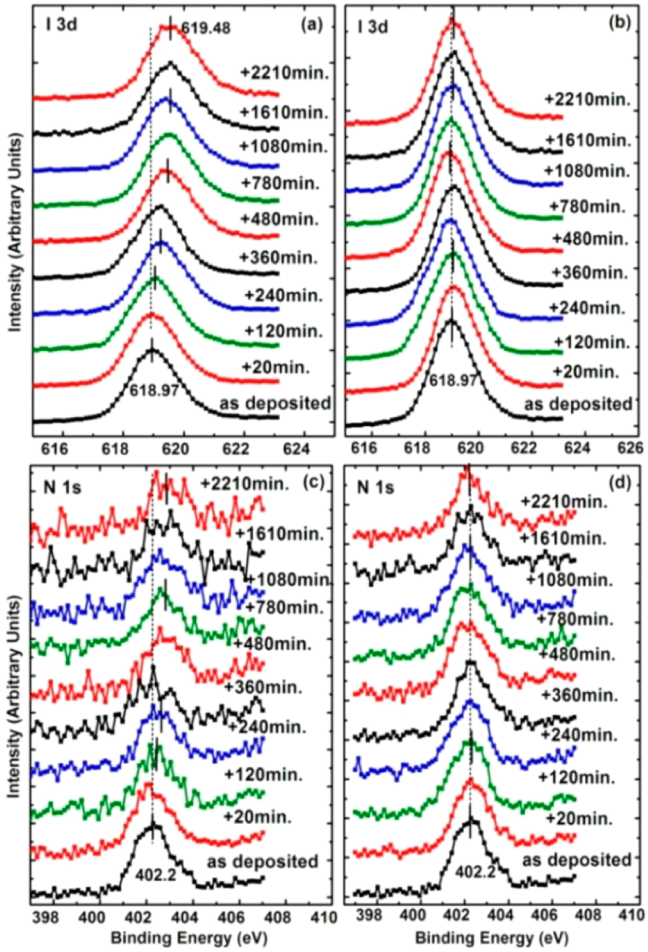

Figure 4. XPS spectra of I 3d and N 1s of the $CH_3NH_3PbI_3$ film at (a, c) laser irradiated positions and (b, d) nonirradiated positions.

of degradation. First, $CH_3NH_3PbI_3$ decomposed into PbI_2 and other volatile components, and then PbI_2 further decomposed into metallic Pb and I. The proposed degradation procedure can be expressed as the following:

$$CH_3NH_3PbI_3 \xrightarrow{\text{light}} (-CH_2-) + NH_3 + HI + PbI_2 \quad (1)$$

$$PbI_2 \xrightarrow{\text{light}} Pb + I_2 \quad (2)$$

The volatile components, NH_3 and HI should fly away from the surface, and so should the iodine by sublimation, leaving unreacted $CH_3NH_3PbI_3$, metallic Pb, and carbon hydrocarbonaceous species on the surface. Without a means of stabilizing the hybrid perovskite thin film, the degradation will severely limit the ability of this material to be used in the consumer market as a light absorbing layer in a solar cell.

The detailed curve fitting of Pb $4f_{7/2}$ is shown in Figure 5a. The dotted line and short bars clearly show the appearance of metallic Pb at 136.87 eV and the 0.46 eV shift of perovskite Pb $4f_{7/2}$ toward higher binding energy. It is clear that the shift of the perovskite Pb $4f_{7/2}$ was already saturated after about 480 min of irradiation, in contrast to the stationary metallic one. Shown in Figure 5b is a plot of the ratio between metallic Pb and total Pb during the laser irradiation, which is calculated from the areas under the fitted curves. A select number of fitted Pb $4f_{7/2}$ curves are shown in Figure 5a. It increased from 26% after 120 min to 33% after 480 min of irradiation, and then the

DOI: 10.1021/acs.jpcc.6b11853
J. Phys. Chem. C 2017, 121, 3904−3910

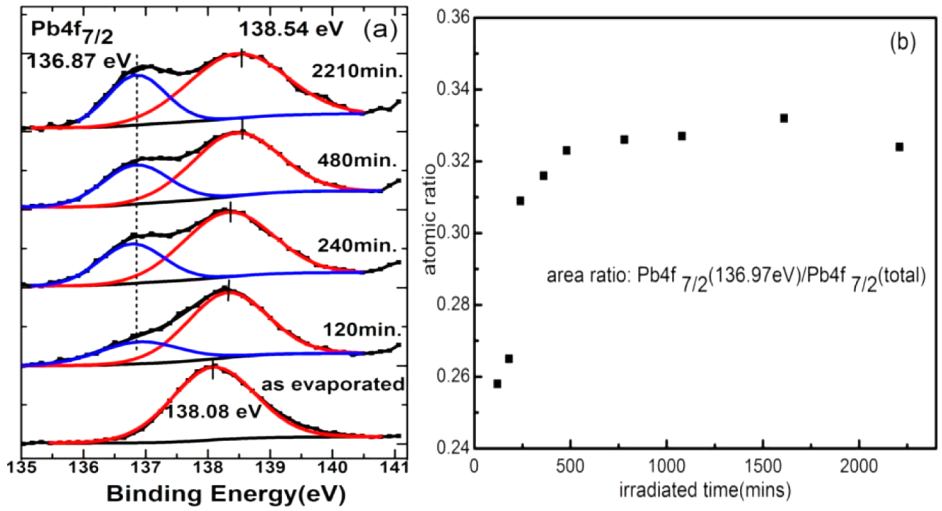

Figure 5. (a) Pb $4f_{7/2}$ decomposition and (b) metallic Pb fraction during laser irradiation.

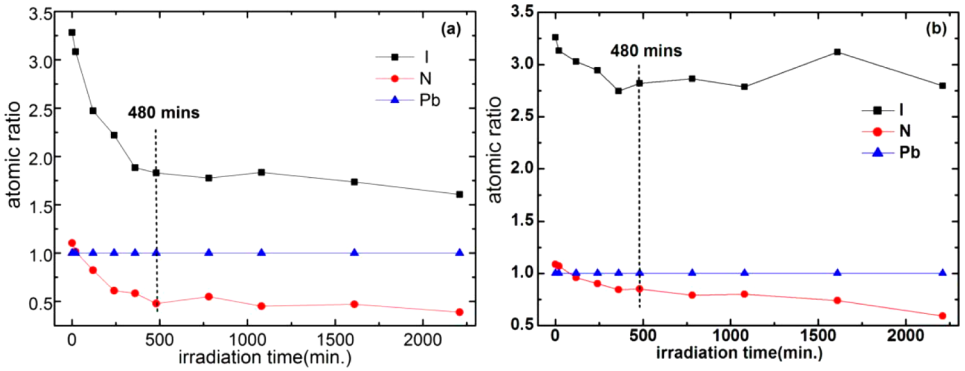

Figure 6. Atomic ratio change of (a) laser irradiated position and (b) nonirradiated position.

ratio remained almost constant. This indicated that the degradation saturated after laser irradiation of about 480 min.

Parts a and b of Figure 6 show the atomic ratio change of the laser irradiated position and the nonirradiated position, respectively. For the laser exposed position, the ratio of N and I decreased quickly, from N:I:Pb = 1.10:3.28:1.00 to 0.48:1.82:1.00 after 480 min of irradiation, at which point the ratios became relatively constant. For the nonexposed position, the ratio of N and I also decreased slightly, from N:I:Pb = 1.09:3.26:1.00 to 0.85:2.82:1.00 at the time corresponding to 480 min of irradiation. The small reduction of the N-to-Pb ratio at the nonirradiated position is likely to be caused by the probing X-ray used for XPS. Reduction by extended exposure to vacuum can be ruled out as we further checked a new position on the sample that was neither irradiated by laser or X-ray after the laser exposure measurements, and found that the atomic ratio to be N:I:Pb = 1.03:3.27:1.00, which was almost the same as the initial ones of laser irradiated and nonirradiated position.

The amount of reduction of N and I by laser radiation alone can be calculated by comparing the ratios of irradiated and nonirradiated positions presented in Figure 6. The N ratio is reduced by 0.38 and that of I is 1.02 by 480 min of laser irradiation after eliminating the contribution from the probing X-ray. Given the stoichiometric ratio of $CH_3NH_3PbI_3$ and that the metallic Pb is now 33% of the total, we can deduce that within the uncertainty of the measurement, about 33% of the $CH_3NH_3PbI_3$ is decomposed at saturation, and all the volatile components left the surface as described in eqs 1 and 2. The total light fluence is 1.96×10^8 J/m^2 at the saturation. The reason for the saturation may be that the exciton quenching centers formed by the metallic lead have effectively quenched all the excitons in the thin film. The formation of the metallic lead requires the sublimation of volatile components, which is kinematically limited by the diffusion process. The decomposition process is then expected to start from the very surface of the $CH_3NH_3PbI_3$ film.

If we take a simplified model that the outer layer is completely decomposed while the underlying one remains intact, we can estimate the thickness of the decomposed layer, which gives the lower limit of the decomposed region. From the exponential attenuation, the XPS intensity I_d from a given thickness d is

$$I_d = \int_0^d I_0 e^{-x/\lambda} \, d_x = I_0\lambda(1 - e^{-d/\lambda}) \tag{3}$$

where I_0 corresponds to the unit emission intensity density and λ the electron mean free path.

The ratio of the intensity from the decomposed layer of thickness d_1 to that of the whole layer of thickness d is given by

$$\frac{I_{d1}}{I_d} = \frac{1 - e^{-d1/\lambda}}{1 - e^{-d/\lambda}} \tag{4}$$

We can deduce that

DOI: 10.1021/acs.jpcc.6b11853
J. Phys. Chem. C 2017, 121, 3904−3910

$$d_1 = -\lambda \ln\left[1 - \frac{I_{d1}}{I_d}(1 - e^{-d/\lambda})\right] \quad (5)$$

With d = 10 nm (the film thickness), λ = 2.0 nm, and the intensity ratio of metallic Pb and the total Pb, I_{d1}/I_d = 0.33, the degradation thickness d_1 caused by laser irradiation is calculated to be 0.82 nm. It should be mentioned that eqs 3−5 are truly valid only for thin films of homogeneous thickness and composition. As the degradation alters the morphology of the film as shown in Figure 1, the degradation thickness thus obtained can only be taken as a rough estimate. Our results may also explain the discrepancy between the PL investigations of the hybrid perovskite degradation by light. In a layered geometry, the light-induced decomposition is limited to the outer surface and the bulk of the material remains intact, thus giving no spectral shift.[26] On the other hand, nanocrystals of hybrid perovskite have much larger relative surface area, and the light-induced degradation is fast and the PL spectral shift is continuous as the diffusion process is no longer a limiting factor.[27]

A natural question is whether the changes by irradiation reported here are due to heating by the laser beam, as hybrid perovskites are known to be unstable above 85 °C even in inert atmosphere.[34] We have carefully analyzed such a possibility and found it unlikely. In our estimate, the gold layer (100 nm) on the silicon substrate acted as a thermal reservoir for the thin $CH_3NH_3PbI_3$ film and should have prevented any appreciable heating and corresponding heating degradation despite hybrid perovskite's extremely low thermal conductance. Following Abbott's model for the heating effects due to a low power CW laser as we used in the experiment, we calculated a steady state temperature increase of less than 1 K.[35] We want to point out that the temperature increase is small because the film is very thin, and appreciable heating may be possible in thicker films or single crystals.[35,36] The calculation demonstrates that the decomposition was caused by the irradiation instead of laser heating effects.

CONCLUSIONS

We have investigated the effects of laser irradiation on evaporated $CH_3NH_3PbI_3$ thin films. After exposing to irradiation for only 120 min by a blue laser with a wavelength of 408 nm and illumination intensity of 6.8×10^{-3} W/mm^2, the film began to decompose. The VBM and the core level were seen to shift toward higher binding energies, indicating an n-type doping during the irradiation. The appearance of metallic Pb and the intensity reduction of N and I demonstrate that the film had decomposed by the laser irradiation. The decomposition saturated after about 480 min of laser irradiation. At saturation, the ratio between metallic Pb and total Pb was about 33%. Correspondingly, N and I were also seen to be reduced by the same fraction due to the laser irradiation. A model of the decomposition is proposed and a lower limit estimate sets the decomposition at approximately 1 nm of the total 10 nm thick film. SEM shows that the surface was roughened and parts of the substrate were uncovered after irradiation because of the stress change caused by the degradation. This research indicates that light can cause and accelerate the decomposition of $CH_3NH_3PbI_3$ films. It also indicates that keeping the volatile decomposition products from leaving the surface is necessary for the long-term application of hybrid perovskite solar cells.

ASSOCIATED CONTENT

Supporting Information

The Supporting Information is available free of charge on the ACS Publications website at DOI: 10.1021/acs.jpcc.6b11853.

More XPS survey scans after irradiation of the sample (PDF)

AUTHOR INFORMATION

Corresponding Author

*(Y.G.) E-mail: ygao@pas.rochester.edu.

ORCID

Youzhen Li: 0000-0001-8994-3627

Jinsong Huang: 0000-0002-0509-8778

Notes

The authors declare no competing financial interest.

ACKNOWLEDGMENTS

The authors would like to acknowledge the support of the National Science Foundation, Grant Nos. CBET-1437656 and DMR-1303742. Y.L and X.X acknowledge the support of China Scholarship Council. J.H acknowledges the financial support from National Science Foundation under the award of Grant OIA-1538893. Technical support from the Nanocenter at the University of Rochester was highly appreciated.

REFERENCES

(1) Li, G.; Zhu, R.; Yang, Y. Polymer Solar Cells. *Nat. Photonics* **2012**, *6*, 153−161.

(2) Yella, A.; Lee, H. W.; Tsao, H. N.; Yi, C. Y.; Chandiran, A. K.; Nazeeruddin, M. K.; Diau, E. W. G.; Yeh, C. Y.; Zakeeruddin, S. M.; Grätzel, M. Porphyrin-Sensitized Solar Cells with Cobalt (II/III)-Based Redox Electrolyte Exceed 12% Efficiency. *Science* **2011**, *334*, 629−634.

(3) Rath, A. K.; Bernechea, M.; Martinez, L.; de Arquer, F. P. G.; Osmond, J.; Konstantatos, G. Solution-Processed Inorganic Bulk Nano-Heterojunctions and Their Application to Solar Cells. *Nat. Photonics* **2012**, *6*, 529−534.

(4) Abrusci, A.; Stranks, S. D.; Docampo, P.; Yip, H.-L.; Jen, A.K.-Y.; Snaith, H. J. High-Performance Perovskite-Polymer Hybrid Solar Cells via Electronic Coupling with Fullerene Monolayers. *Nano Lett.* **2013**, *13* (7), 3124−3128.

(5) Kim, H.-S.; Lee, C.-R.; Im, J.-H.; Lee, K.-B.; Moehl, T.; Marchioro, A.; Moon, S.-J.; Humphry -Baker, R.; Yum, J.-H.; Moser, J. E. Lead Iodide Perovskite Sensitized All-Solid-State Submicron Thin Film Mesoscopic Solar Cell with Efficiency Exceeding 9%. *Sci. Rep.* **2012**, *2*, 591.

(6) Dunlap-Shohl, W. A.; Younts, R.; Gautam, B.; Gundogdu, K.; Mitzi, D. B. Effects of Cd Diffusion and Doping in High-Performance Perovskite Solar Cells Using CdS as Electron Transport Layer. *J. Phys. Chem. C* **2016**, *120*, 16437−16445.

(7) Xie, H. P.; Liu, X. L.; Lyu, L.; Niu, D. M.; Wang, Q.; Huang, J. S.; Gao, Y. L. Effects of Precursor Ratios and Annealing on Electronic Structure and Surface Composition of CH(3)NH(3)PbI(3) Perovskite Films. *J. Phys. Chem. C* **2016**, *120*, 215−220.

(8) Yang, W. S.; Noh, J. H.; Jeon, N. J.; Kim, Y. C.; Ryu, S.; Seo, J.; Seok, S. I. High-Performance Photovoltaic Perovskite Layers Fabricated Through Intramolecular Exchange. *Science* **2015**, *348*, 1234−1237.

(9) Zhou, H. P.; Chen, Q.; Li, G.; Luo, S.; Song, T. B.; Duan, H. S.; Hong, Z. R.; You, J. B.; Liu, Y. S.; Yang, Y. Interface Engineering of Highly Efficient Perovskite Solar Cells. *Science* **2014**, *345*, 542−546.

(10) Kojima, A.; Teshima, K.; Shirai, Y.; Miyasaka, T. Organometal Halide Perovskites as Visible-Light Sensitizers for Photovoltaic Cells. *J. Am. Chem. Soc.* **2009**, *131*, 6050.

DOI: 10.1021/acs.jpcc.6b11853
J. Phys. Chem. C 2017, 121, 3904−3910

(11) Ball, J. M.; Lee, M. M.; Hey, A.; Snaith, H. J. Low-Temperature Processed Meso-Superstructured to Thin-Film Perovskite Solar Cells. *Energy Environ. Sci.* **2013**, *6*, 1739−1743.
(12) National Renewable Energy Laboratory,Best Research-Cell Efficiencies. http://www.nrel.gov/ncpv/images/efficiency_chart.jpg (accessed April, 2016).
(13) Liu, X. L.; Wang, C. G.; Lyu, L.; Wang, C. C.; Xiao, Z. G.; Bi, C.; Huang, J. S.; Gao, Y. L. Electronic Structures at the Interface Between Au and $CH_3NH_3PbI_3$. *Phys. Chem. Chem. Phys.* **2015**, *17*, 896−902.
(14) Wang, C. G.; Wang, C. C.; Liu, X. L.; Kauppi, J.; Shao, Y. C.; Xiao, Z. G.; Bi, C.; Huang, J. S.; Gao, Y. L. Electronic Structure Evolution of Fullerene on $CH_3NH_3PbI_3$. *Appl. Phys. Lett.* **2015**, *106*, 111603.
(15) Wang, C. G.; Liu, X. L.; Wang, C. C.; Xiao, Z. G.; Bi, C.; Shao, Y. C.; Huang, J. S.; Gao, Y. L. Surface Analytical Investigation on Organometal Triiodide Perovskite. *J. Vac. Sci. Technol., B: Nanotechnol. Microelectron.: Mater., Process., Meas., Phenom.* **2015**, *33*, 032401.
(16) Bi, C.; Shao, Y. C.; Yuan, Y. B.; Xiao, Z. G.; Wang, C. G.; Gao, Y. L.; Huang, J. S. Understanding the Formation and Evolution of Interdiffusion Grown Organolead Halide Perovskite Thin Films by Thermal Annealing. *J. Mater. Chem. A* **2014**, *2*, 18508−18514.
(17) Schulz, P.; Edri, E.; Kirmayer, S.; Hodes, G.; Cahen, D.; Kahn, A. Interface Energetics in Organo-Metal Halide Perovskite-Based Photovoltaic Cells. *Energy Environ. Sci.* **2014**, *7*, 1377−1381.
(18) Wang, Q.; Shao, Y. C.; Xie, H. P.; Lyu, L.; Liu, X. L.; Gao, Y. L.; Huang, J. S. Qualifying Composition Dependent p and N Self-Doping in $CH_3NH_3PbI_3$. *Appl. Phys. Lett.* **2014**, *105*, 163508.
(19) Xiao, Z. G.; Bi, C.; Shao, Y. C.; Dong, Q. F.; Wang, Q.; Yuan, Y. B.; Wang, C. G.; Gao, Y. L.; Huang, J. S. Efficient, High Yield Perovskite Photovoltaic Devices Grown by Interdiffusion of Solution-Processed Precursor Stacking Layers. *Energy Environ. Sci.* **2014**, *7*, 2619−2623.
(20) Liu, M. Z.; Johnston, M. B.; Snaith, H. J. Efficient Planar Heterojunction Perovskite Solar Cells by Vapour Deposition. *Nature* **2013**, *501*, 395−398.
(21) Wang, C. C.; Li, Y. Z.; Xu, X. M.; Wang, C. G.; Xie, F. Y.; Gao, Y. L. Degradation of Co-Evaporated Perovskite Thin Film in Air. *Chem. Phys. Lett.* **2016**, *649*, 151−155.
(22) Li, Y. Z.; Xu, X. M.; Wang, C. G.; Wang, C. C.; Xie, F. Y.; Yang, J. L.; Gao, Y. L. Degradation by Exposure of Coevaporated $CH_3NH_3PbI_3$ Thin Films. *J. Phys. Chem. C* **2015**, *119*, 23996−24002.
(23) Leijtens, T.; Eperon, G. E.; Pathak, S.; Abate, A.; Lee, M. M.; Snaith, H. J. Overcoming Ultraviolet Light Instability of Sensitized TiO_2 with Meso-Superstructured Organometal Tri-Halide Perovskite Solar Cells. *Nat. Commun.* **2013**, *4*, 2885.
(24) Murugadoss, G.; Tanaka, S.; Mizuta, G.; Kanaya, S.; Nishino, H.; Umeyama, T.; Imahori, H.; Ito, S. Light Stability Tests of Methylammonium and Formamidinium Pb-Halide Perovskites for Solar Cell Applications. *Jpn. J. Appl. Phys.* **2015**, *54*, 08KF08.
(25) Bryant, D.; Aristidou, N.; Pont, S.; Sanchez-Molina, I.; Chotchunangatchaval, T.; Wheeler, S.; Durrant, J. R.; Haque, S. A. Light and Oxygen Induced Degradation Limits the Operational Stability of Methylammonium Lead Triiodide Perovskite Solar Cells. *Energy Environ. Sci.* **2016**, *9*, 1655−1660.
(26) Yuan, H. F.; Debroye, E.; Janssen, K.; Naiki, H.; Steuwe, C.; Lu, G.; Moris, M.; Orgiu, E.; Uji-i, H.; De Schryver, F.; et al. Degradation of Methylammonium Lead Iodide Perovskite Structures through Light and Electron Beam Driven Ion Migration. *J. Phys. Chem. Lett.* **2016**, *7*, 561−566.
(27) Merdasa, A.; Bag, M.; Tian, Y. X.; Källman, E.; Dobrovolsky, A.; Scheblykin, I. G. Super-Resolution Luminescence Microspectroscopy Reveals the Mechanism of Photoinduced Degradation in $CH_3NH_3PbI_3$ Perovskite Nanocrystals. *J. Phys. Chem. C* **2016**, *120*, 10711−10719.
(28) Li, Y. Z.; Xu, X. M.; Wang, C. G.; Wang, C. C.; Xie, F. Y.; Yang, J. L.; Gao, Y. L. Investigation on Thermal Evaporated $CH_3NH_3PbI_3$ Thin Films. *AIP Adv.* **2015**, *5*, 097111.
(29) Niu, G. D.; Li, W. Z.; Meng, F. Q.; Wang, L. D.; Dong, H. P.; Qiu, Y. Study on the Stability of $CH_3NH_3PbI_3$ Films and the Effect of Post-Modification by Aluminum Oxide in All-Solid-State Hybrid Solar Cells. *J. Mater. Chem. A* **2014**, *2*, 705−710.
(30) Patnaik, P. *Handbook of Inorganic Chemicals*. McGraw-Hill Press: New York, 2003.
(31) Lindblad, R.; Jena, N. K.; Philippe, B.; Oscarsson, J.; Bi, D. Q.; Lindblad, A.; Mandal, S.; Pal, B.; Sarma, D. D.; Karis, O.; et al. Electronic Structure of $CH_3NH_3PbX_3$ Perovskites: Dependence on the Halide Moiety. *J. Phys. Chem. C* **2015**, *119*, 1818−1825.
(32) Conings, B.; Baeten, L.; De Dobbelaere, C.; D'Haen, J.; Manca, J.; Boyen, H. G. Perovskite-Based Hybrid Solar Cells Exceeding 10% Efficiency with High Reproducibility Using a Thin Film Sandwich Approach. *Adv. Mater.* **2014**, *26*, 2041−2046.
(33) Sadoughi, G.; Starr, D. E.; Handick, E.; Stranks, S. D.; Gorgoi, M.; Wilks, R. G.; Baer, M.; Snaith, H. J. Observation and Mediation of the Presence of Metallic Lead in Organic-Inorganic Perovskite Films. *ACS Appl. Mater. Interfaces* **2015**, *7*, 13440−13444.
(34) Conings, B.; Drijkoningen, J.; Gauquelin, N.; Babayigit, A.; D'Haen, J.; D'Olieslaeger, L.; Ethirajan, A.; Verbeeck, J.; Manca, J.; Mosconi, E.; et al. Intrinsic Thermal Instability of Methylammonium Lead Trihalide Perovskite. *Adv. Energy Mater.* **2015**, *5*, 1500477.
(35) Abbott, D.; Davis, B.; Gonzalez, B.; Hernandez, A.; Eshraghian, K. Modelling of Low Power CW Laser Beam Heating Effects on A GaAs Substrate. *Solid-State Electron.* **1998**, *42*, 809−816.
(36) Pisoni, A.; Jaćimović, J.; Barišić, O. S.; Spina, M.; Gaál, R.; Forró, L.; Horváth, E. Ultra-Low Thermal Conductivity in Organic-Inorganic Hybrid Perovskite $CH_3NH_3PbI_3$. *J. Phys. Chem. Lett.* **2014**, *5*, 2488−2492.

DOI: 10.1021/acs.jpcc.6b11853
J. Phys. Chem. C 2017, 121, 3904−3910